A Non-Stationary Wideband Channel Model for Massive MIMO Communication Systems

Shangbin Wu, Cheng-Xiang Wang, *Senior Member, IEEE*, Harald Haas, *Member, IEEE*,
el-Hadi M. Aggoune, *Senior Member, IEEE*, Mohammed M. Alwakeel, *Senior Member, IEEE*, and
Bo Ai, *Senior Member, IEEE*

Abstract—This paper proposes a novel non-stationary wideband multi-confocal ellipse two dimensional (2-D) channel model for massive multiple-input multiple-output (MIMO) communication systems. Spherical wavefront is assumed in the proposed channel model, instead of the plane wavefront assumption used in conventional MIMO channel models. In addition, the birth-death process is incorporated into the proposed model to capture the dynamic properties of clusters on both the array and time axes. Statistical properties of the channel model such as the space-time-frequency correlation function and power imbalance on the antenna array are studied. The impact of the spherical wavefront assumption on the statistical properties of the channel model is investigated. Furthermore, numerical analysis shows that the proposed channel model is able to capture specific characteristics of massive MIMO channel as observed in measurements.

Index Terms—Massive MIMO, multi-confocal ellipse channel model, spherical wavefront, non-stationarity, birth-death process.

S. Wu and C.-X. Wang are with the Joint Research Institute for Signal and Image Processing, School of Engineering and Physical Sciences, Heriot-Watt University, Edinburgh EH14 4AS, U.K., and also with the Sensor Networks and Cellular Systems (SNCS) Research Center, University of Tabuk, Tabuk 47315/4013, Saudi Arabia. C.-X. Wang is also with the School of Information Science and Engineering, Shandong University, Jinan, Shandong 250100, China (e-mail: sw271@hw.ac.uk; cheng-xiang.wang@hw.ac.uk).

H. Haas is with the Joint Research Institute for Signal and Image Processing, School of Engineering, University of Edinburgh, Edinburgh EH9 3JL, U.K. (e-mail: h.haas@ed.ac.uk).

e.-H. M. Aggoune and M. M. Alwakeel are with the Sensor Networks and Cellular Systems (SNCS) Research Center, University of Tabuk, Tabuk 47315/4013, Saudi Arabia (e-mail: haggoune.sncs@ut.edu.sa; alwakeel@ut.edu.sa).

B. Ai is with the State Key Laboratory of Rail Traffic Control and Safety, Beijing Jiaotong University, Beijing 100044, China, and also with the Engineering University of Armed Police Force, Xi'an 710086, China (e-mail: boai@bjtu.edu.cn).

Color versions of one or more of the figures in this paper are available online at http://ieeexplore.ieee.org.

Digital Object Identifier 10.1109/TWC.2014.2366153

I. INTRODUCTION

MULTIPLE-input multiple-output (MIMO) technology has been attracting researchers' attention for its capability of providing improved link reliability and system capacity without extra spectral resources [1]. MIMO has been deployed in a number of advanced wireless communication systems such as Worldwide Interoperability for the Microwave Access (WiMAX) [2] and the Long Term Evolution (LTE). The latest LTE standard (Release-12) [3], for instance, can support up to 8-layer transmission which is equivalent to at least 8 antennas at the base station (BS) and 8 antennas at the mobile station (MS).

A massive MIMO system is equipped with much more antennas, typically tens or hundreds, than conventional MIMO systems [4]–[7]. With such a massive number of antennas, it has been demonstrated that a massive MIMO system is able to provide many benefits, such as greatly increasing the capacity, simplifying scheduling design in the frequency domain [4], and averaging interference according to the large number theorem [5]. Generally speaking, a massive MIMO system can be considered as an enhanced version of conventional MIMO by utilizing an enormous number of antennas. As a result, its system performance, in terms of capacity, efficiency, and reliability, is significantly better than conventional MIMO systems [4]–[7].

To design and evaluate MIMO systems, an accurate small-scale fading MIMO channel model is necessary. Conventional small-scale fading MIMO channel models have been widely studied in the literature. Extensive geometry-based stochastic models (GBSMs) for conventional MIMO channels known as one-ring model, two-ring model, and ellipse model can be found in [8]–[12]. Also, a combined ellipse and two-ring model was proposed in [13] and [14], a multiple circular-ring model was proposed in [15], and three-dimensional (3-D) concentric-cylinder models can be found in [16] and [17]. The authors in [18] proposed a twin-cluster model which concerned only the first and the last bounces. The spatial channel model (SCM) [19], WINNER II model [20], IMT-A model [21], COST 273 model [22], and COST 2100 model [23], [24] have also been widely utilized. Besides, correlation-based conventional MIMO channel models such as the Kronecker model and the Weichselberger model were used to investigate the performance of massive MIMO systems in [25] and [26].

However, according to the measurement observations in [27] and [28], the above mentioned MIMO channel models [8]–[26] are not sufficient to accurately capture certain characteristics of massive MIMO channels. First, conventional MIMO channel

models solely assume that the distance between a scatterer and an antenna array is far beyond the Rayleigh distance [29], [30], i.e., $2\mathcal{M}^2/\lambda$, where $\mathcal{M}$ is the dimension of the antenna array and λ is the carrier wavelength. Namely, the farfield and plane wavefront assumptions were usually applied to simplifying the channel models. However, the authors in [27] and [28] stated that as the number of antennas is massive, the plane wavefront assumption is not fulfilled for massive MIMO channels. Instead, a spherical wavefront channel model should be considered. Spherical wavefront models and plane wavefront models were compared in [31] and [32]. The authors in [31] pointed out that the plane wavefront assumption underestimates the rank of the channel matrix. However, [31] and [32] only focused on short range or constant distance communications which were not applicable for general massive MIMO systems. Second, dynamic properties of clusters such as cluster appearance and disappearance, angle of arrival (AoA) shifts, as well as non-stationarities were observed on the antenna array axis [27], [28]. The characterization of non-stationarities was investigated in [33]–[36], where the appearance and disappearance of clusters on the time axis were modeled using the birth-death or Markov processes. The authors in [37] and [38] analyzed time-variant geometrical properties such as AoA and angles of departure (AoD), but they ignored the evolution of clusters. However, [33]–[38] only took non-stationarities on the time axis into account and ignored non-stationarities on the array axis. The authors in [39] considered nearfield effects and non-stationarities on the array axis. However, in [39], the impact of spherical wavefront on non line-of-sight (NLOS) components was missing, characteristics of cluster appearance and disappearance were not studied in detail, and non-stationarities on the time axis were not included. A 3-D non-stationary twin-cluster channel model was proposed in [40] for massive MIMO systems considering spherical wavefront and non-stationarities on both time and array axes. However, AoAs and AoDs were assumed independent, channel characteristics such as power imbalance on the antenn array and space-time-frequency correlation function (STFCF) were not investigated in [40].

In this paper, a novel two dimensional (2-D) non-stationary wideband multi-confocal ellipse model for massive MIMO channels is proposed. This channel model is developed to capture the spherical wavefront effect and non-stationary properties on both the array and time axes. Also, AoAs and AoDs are assumed dependent in the ellipse model. The major **contributions** of this paper are summarized as follows:

1) The plane wavefront assumption for conventional MIMO channel models is relaxed, i.e., the nearfield effect of spherical wavefront is considered in the proposed wideband ellipse model. The impacts of spherical wavefront assumption on both the line-of-sight (LOS) component and NLOS components are studied.

2) Birth-death process is applied to the array axis to capture the cluster appearance and disappearance on the antenna array axis as reported in [27]. Combining the birth-death process modeling cluster time evolution in [33], array-time evolution of clusters of the proposed wideband massive MIMO channel model is proposed. A novel cluster
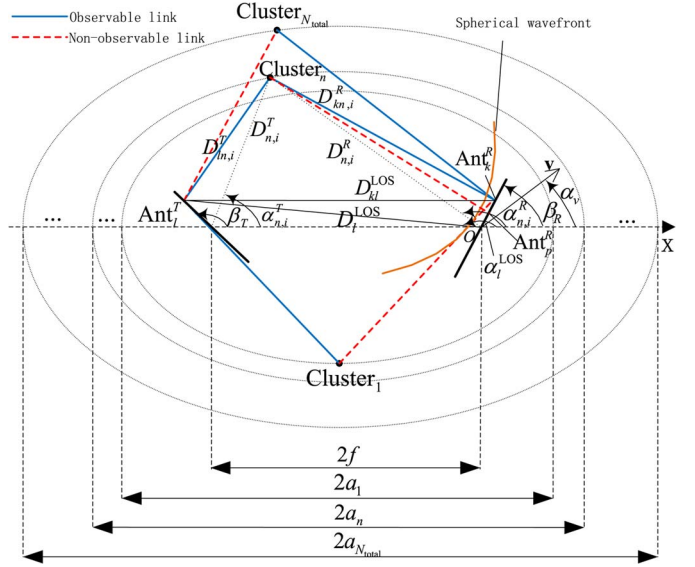

Fig. 1. A wideband multi-confocal ellipse model for massive MIMO systems.

evolution algorithm is developed based on the birth-death process on both the array and time axes.

3) Statistical properties of the proposed massive MIMO channel model such as STFCF and cumulative distribution functions (CDFs) of survival probabilities of clusters and received power imbalance on the antenna array are investigated.

This paper is organized as follows. In Section II, the proposed wideband ellipse MIMO channel model is discussed in detail. This includes geometrical properties derived under the spherical wavefront assumption as well as the novel algorithm which describes the cluster evolution on the array axis. Section III presents the array-time evolution model, which describes dynamic properties of clusters on both the array and time axes. Statistical properties are investigated as well. In Section IV, numerical analysis is given. Conclusions are finally drawn in Section V.

II. A WIDEBAND ELLIPSE MODEL FOR MASSIVE MIMO SYSTEMS

In this section, a novel wideband ellipse 2-D channel model for massive MIMO is proposed, including spherical wavefront and cluster evolution on the array axis as shown in Fig. 1. (The combination of cluster evolutions on both the time and array axes will be presented in Section III). Let us assume that the transmitter and receiver are equipped with uniform linear arrays (ULAs) with M_T and M_R omnidirectional antennas, respectively. The antenna elements are spaced with separation δ_T and δ_R, and they are located at the focal points of the confocal ellipses with a distance of $2f$. Let Ant_l^T represent the l-th antenna of the transmit array and Ant_k^R represent the k-th antenna of the receive array. The n-th cluster is on the n-th ellipse with major axis $2a_n$. The angle $\beta_T(\beta_R)$ denotes the tilt angle of the transmit (receive) antenna array. The angle α_v denotes the angle between the x-axis and the direction of movement of the receiver. The maximum Doppler frequency and carrier wavelength are denoted as $f_{\max}$ and λ, respectively.

TABLE I
SUMMARY OF KEY PARAMETER DEFINITIONS.

$\delta_T(\delta_R)$	antenna spacing of the transmit (receive) antenna array
$M_T(M_R)$	number of transmit (receive) antennas
$2f$	distance between the transmitter and receiver (focal length)
a_n	semi-major axis of the n-th ellipse
$\beta_T(\beta_R)$	title angles of the transmit (receive) antenna array
$f_{\max}, \lambda$	maximum Doppler frequency and carrier wavelength
$\text{Ant}_l^T, \text{Ant}_k^R$	the l-th transmit antenna and the k-th receive antenna
D_{kl}^{LOS}	LOS distance between k-th receive antenna and the l-th transmit antenna
$D_{ln,i}^T$	distance between the n-th cluster and the l-th transmit antenna via the i-th ray within the cluster
$D_{kn,i}^R$	distance between the n-th cluster and the k-th receive antenna via the i-th ray within the cluster
f_{kl}^{LOS}	Doppler frequency of the LOS component between k-th receive antenna and the l-th transmit antenna
$f_{n,i}$	Doppler frequency of the n-cluster via the i-th ray
$\varphi_{kl}^{\text{LOS}}$	phase of the LOS component between k-th receive antenna and the l-th transmit antenna
$\varphi_{kl,n,i}$	phase of the n-th cluster between k-th receive antenna and the l-th transmit antenna via the i-th ray
$\alpha_{n,i}^T$	AoD of the i-th ray of the n-th cluster to the transmit array center
$\alpha_{n,i}^R$	AoA of the i-th ray of the n-th cluster to the receive array center

For massive MIMO channel models, there are two important properties should be noticed. First, the farfield assumption for conventional MIMO channel models [8], [13], which is equivalent to the plane wavefront assumption, is not fulfilled as the dimension of the antenna array can not be ignored when the number of antennas is massive. As a result, the wavefront emitted from the n-th cluster to the receive array is assumed to be spherical as shown in Fig. 1. Then, the AoA is no longer linear along the array, and it needs to be computed based on geometrical relationships. The impact of spherical wavefront will be analyzed in detail in following paragraphs.

Second, as reported in [27] and [28], the behavior of clusters is not stationary on the array axis, which means that a cluster may not always be observable to all the antenna elements of an array in conventional MIMO channel models. An example is given in Fig. 1 that Cluster$_1$ is observable to Ant_l^T but it is not observable to Ant_k^R. Cluster$_{N_{\text{total}}}$ is observable to Ant_k^R but it is non-observable to Ant_l^T. Conversely, Cluster$_n$ is observable to both Ant_k^R and Ant_l^T but not to Ant_p^R. These situations imply that *different antenna elements may observe different sets of clusters*, which is not assumed in conventional MIMO channel models. Let $C_l^T(C_k^R)$ denote the cluster set in which clusters are observable to $\text{Ant}_l^T(\text{Ant}_k^R)$, the generation of C_l^T and C_k^R will be modeled as birth-death processes as described in Section II-A. Also, let N_{total} denote the total number of clusters which are observable to at least one transmit antenna and one receive antenna, N_{total} can be expressed as [40]

$$N_{\text{total}} = \text{card}\left(\bigcup_{l=1}^{M_T}\bigcup_{k=1}^{M_R}\left(C_l^T(t)\bigcap C_k^R(t)\right)\right) \quad (1)$$

where the operator $\text{card}(\cdot)$ denotes the cardinality of a set. Then, a cluster, say Cluster$_n(n \leqslant N_{\text{total}})$, is observable to both Ant_l^T and Ant_k^R if and only if Cluster$_n \in \{C_l^T \cap C_k^R\}$.

Based on the above mentioned analysis and the summary of key parameter definitions in Table I, the wideband massive MIMO channel can be presented as an $M_R \times M_T$ complex matrix $\mathbf{H}(t,\tau) = [h_{kl}(t,\tau)]_{M_R \times M_T}$, where $k = 1, 2, \cdots, M_R$ and $l = 1, 2, \cdots, M_T$. Next, assume the initial phase of the signal at the transmitter is φ_0, LOS Rician factor is K and the LOS component is always connected to all antennas and the first cluster to arrive at the receiver if the LOS component exists.

Additionally, assume that the mean power of the n-th cluster is P_n and there are S rays within one cluster and $\alpha_{n,i}^R$ is the AoA of the i-th ray of the n-th cluster to the receive array center, $\alpha_{n,i}^T$ is the AoD of the i-th ray of the n-th cluster $(i = 1, 2, \cdots, S)$ to the transmit array center, the multipath complex gains $h_{kl}(t,\tau)$ of the theoretical model $(S \to \infty)$ between Ant_l^T and Ant_k^R at delay τ can be presented as

$$h_{kl}(t,\tau) = \sum_{n=1}^{N_{\text{total}}} h_{kl,n}(t)\delta(\tau - \tau_n) \quad (2)$$

where the complex gain $h_{kl,n}(t)$ of Cluster$_n$ can be computed as

— if Cluster$_n \in \{C_l^T \cap C_k^R\}$,

$$h_{kl,n}(t) = \underbrace{\delta(n-1)\sqrt{\frac{K}{K+1}}e^{j\left(2\pi f_{kl}^{\text{LOS}}t+\varphi_{kl}^{\text{LOS}}\right)}}_{\text{LOS}}$$

$$+ \underbrace{\sqrt{\frac{P_n}{K+1}}\lim_{S\to\infty}\frac{1}{\sqrt{S}}\sum_{i=1}^{S}e^{j(2\pi f_{n,i}t+\varphi_{kl,n,i})}}_{\text{NLOS}} \quad (3)$$

— if Cluster$_n \notin \{C_l^T \cap C_k^R\}$,

$$h_{kl,n}(t) = 0. \quad (4)$$

For the LOS component, under the spherical wavefront assumption,

$$\varphi_{kl}^{\text{LOS}} = \varphi_0 + \frac{2\pi}{\lambda}\left[(D_l^{\text{LOS}})^2 + \left(\frac{M_R - 2k + 1}{2}\delta_R\right)^2\right.$$
$$\left. - (M_R - 2k + 1)\delta_R D_l^{\text{LOS}}\cos\left(\alpha_l^{\text{LOS}} - \beta_R\right)\right]^{1/2} \quad (5)$$

where

$$D_l^{\text{LOS}} = \left[(2f)^2 + \left(\frac{M_T - 2l + 1}{2}\delta_T\right)^2\right.$$
$$\left. - 2f(M_T - 2l + 1)\delta_T\cos(\beta_T)\right]^{1/2} \quad (6)$$

and the AoA α_l^{LOS} of the LOS component from Ant_l^T to the receive array center can be computed as

$$\alpha_l^{\text{LOS}} = \pi - \arcsin\left[\frac{\sin\beta_T}{D_l^{\text{LOS}}}\left(\frac{M_T - 2l + 1}{2}\delta_T\right)\right]. \quad (7)$$

The Doppler frequency f_{kl}^{LOS} of the LOS component between Ant_k^R and Ant_l^T can be calculated as

$$f_{kl}^{\text{LOS}} = f_{\max}\cos\left(\pi - \arcsin\left[\frac{D_l^{\text{LOS}}}{D_{kl}^{\text{LOS}}}\sin\left(\alpha_l^{\text{LOS}} - \beta_R\right)\right]\right) \quad (8)$$

where

$$D_{kl}^{\text{LOS}} = \left[\left(D_l^{\text{LOS}}\right)^2 + \left(\frac{M_R - 2k + 1}{2}\delta_R\right)^2\right.$$
$$\left. - (M_R - 2k + 1)\delta_R D_l^{\text{LOS}}\cos\left(\alpha_l^{\text{LOS}} - \beta_R\right)\right]^{1/2}. \quad (9)$$

For the NLOS components, AoAs $\alpha_{n,i}^R$ and AoDs $\alpha_{n,i}^T$ are dependent in an ellipse model, their relationship can be presented as [8]

$$\alpha_{n,i}^T = \begin{cases} g\left(\alpha_{n,i}^R\right) & \text{if } 0 < \alpha_{n,i}^R \leqslant \alpha_0 \\ g\left(\alpha_{n,i}^R\right) + \pi & \text{if } \alpha_0 < \alpha_{n,i}^R \leqslant 2\pi - \alpha_0 \\ g\left(\alpha_{n,i}^R\right) + 2\pi & \text{if } 2\pi - \alpha_0 < \alpha_{n,i}^R \leqslant 2\pi \end{cases} \quad (10)$$

where

$$g(\alpha_{n,i}^R) = \arctan\left[\frac{(k_0^2 - 1)\sin\left(\alpha_{n,i}^R\right)}{2k_0 + (k_0^2 + 1)\cos\left(\alpha_{n,i}^R\right)}\right] \quad (11)$$

$$\alpha_0 = \pi - \arctan\left(\frac{k_0^2 - 1}{2k_0}\right) \quad (12)$$

$$k_0 = a_n/f. \quad (13)$$

Given the semi-major axis a_1 of the first ellipse, a_n can be determined by τ_n relative to the first ellipse as

$$a_n = c\tau_n + a_1 \quad (14)$$

where c is the speed of light. Accordingly, the distance between the n-th cluster and the transmitter via the i-th ray, $D_{n,i}^T$, as well as the distance between the n-th cluster and the receiver via the i-th ray, $D_{n,i}^R$, can be derived according to their geometrical relationships:

$$D_{n,i}^R = \frac{2a_n\sin\alpha_{n,i}^T}{\sin\alpha_{n,i}^T + \sin\left(\pi - \alpha_{n,i}^R\right)} \quad (15)$$

$$D_{n,i}^T = \frac{2a_n\sin\left(\pi - \alpha_{n,i}^R\right)}{\sin\alpha_{n,i}^T + \sin\left(\pi - \alpha_{n,i}^R\right)}. \quad (16)$$

Then, the distance between the n-th cluster and Ant_l^T via the i-th ray within the cluster, $D_{ln,i}^T$, can be computed as

$$D_{ln,i}^T = \left[\left(D_{n,i}^T\right)^2 + \left(\frac{M_T - 2l + 1}{2}\delta_T\right)^2\right.$$
$$\left. - (M_T - 2l + 1)\delta_T D_{n,i}^T\cos\left(\beta_T - \alpha_{n,i}^T\right)\right]^{1/2}. \quad (17)$$

The distance between the n-th cluster and Ant_k^R via the i-th ray within the cluster, $D_{kn,i}^R$, can be computed as

$$D_{kn,i}^R = \left[\left(D_{n,i}^R\right)^2 + \left(\frac{M_R - 2k + 1}{2}\delta_R\right)^2\right.$$
$$\left. - (M_R - 2k + 1)\delta_R D_{n,i}^R\cos\left(\alpha_{n,i}^R - \beta_R\right)\right]^{1/2}. \quad (18)$$

Based on the above equations, the received phase of Ant_k^R via the i-th ray within the n-th cluster from Ant_l^T, $\varphi_{kl,n,i}$, can be expressed as

$$\varphi_{kl,n,i} = \varphi_0 + \frac{2\pi}{\lambda}\left(D_{ln,i}^T + D_{kn,i}^R\right). \quad (19)$$

The Doppler frequency of the i-th ray within the n-th cluster, $f_{n,i}$, is

$$f_{n,i} = f_{\max}\cos\left(\alpha_{n,i}^R - \alpha_v\right). \quad (20)$$

A. Array Axis Evolution—Generation of Cluster Sets C_l^T and C_k^R

Thus far, all the geometrical relationships have been derived from (5) to (20). In this section, we will model the dynamic properties of clusters, i.e., the appearance and disappearance of clusters on the array axis, using a birth-death process. In previous literature [33] and [44], the birth-death process was deployed to model the channel non-stationarity along the time axis, describing the cluster variations in terms of the change of time. For massive MIMO systems, the time axis birth-death process [33] will be adapted to the array axis [40]. Let λ_G (per meter) and λ_R (per meter) denote the cluster generation rate and the recombination rate. Next, by defining the scenario-dependent correlation factor D_c^a on the array axis, let the operator $\xrightarrow{\text{E}}$ represent evolution on either array or time axis, when a cluster set evolves from Ant_{l-1}^T to Ant_l^T or from Ant_{k-1}^R to Ant_k^R, denoted as $C_{l-1}^T \xrightarrow{\text{E}} C_l^T$ or $C_{k-1}^R \xrightarrow{\text{E}} C_k^R$, the survival probabilities of the clusters inside the cluster set at the transmitter P_{survival}^T and at the receiver P_{survival}^R can be modeled as [45]

$$P_{\text{survival}}^T = e^{-\lambda_R \frac{\delta_T}{D_c^a}} \quad (21)$$

$$P_{\text{survival}}^R = e^{-\lambda_R \frac{\delta_R}{D_c^a}}. \quad (22)$$

According to the birth-death process, the duration between two cluster appearances and the duration between two cluster disappearances are exponentially distributed [34], [45], the average number of newly generated clusters N_{new}^T and N_{new}^R based on the Poisson process can be computed as [45]

$$\text{E}\left[N_{\text{new}}^T\right] = \frac{\lambda_G}{\lambda_R}\left(1 - e^{-\frac{\delta_T}{D_c^a}}\right) \quad (23)$$

$$\text{E}\left[N_{\text{new}}^R\right] = \frac{\lambda_G}{\lambda_R}\left(1 - e^{-\frac{\delta_R}{D_c^a}}\right) \quad (24)$$
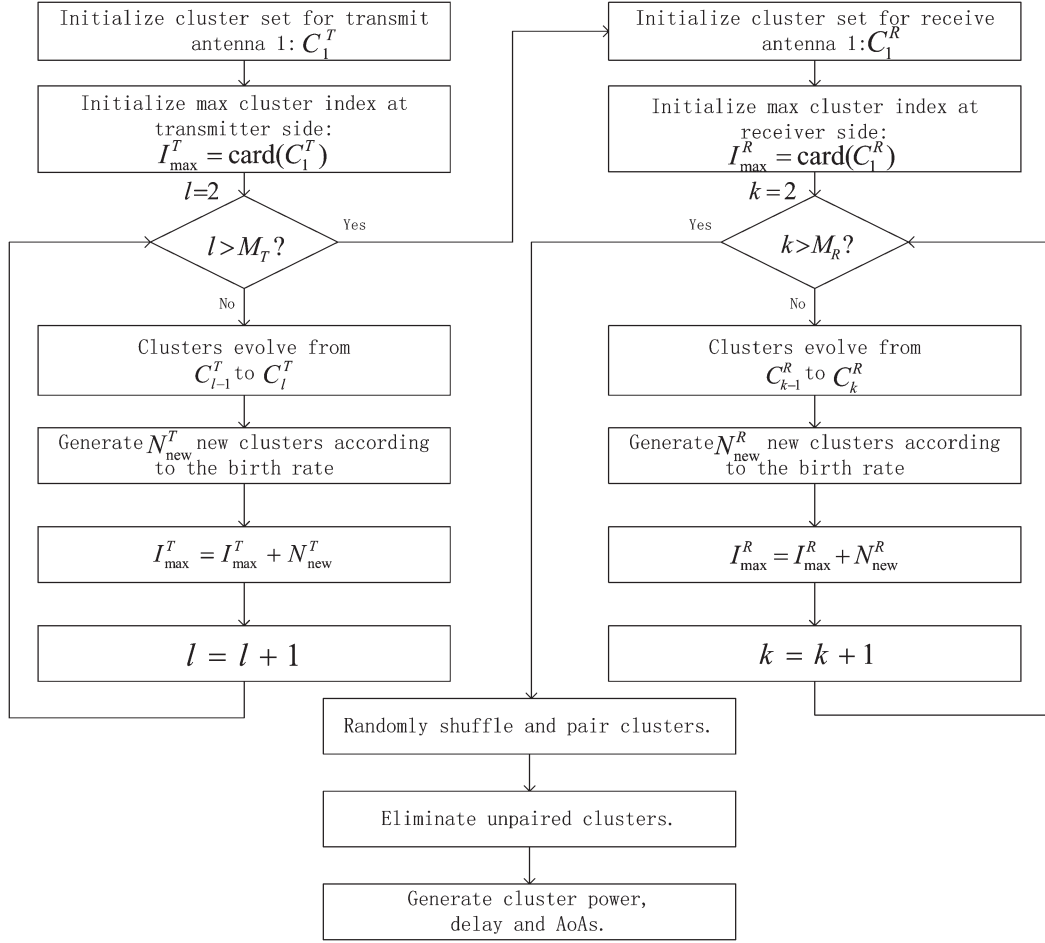
Fig. 2.   Cluster generation algorithm flowchart.

where $E[\cdot]$ designates the expectation. Cluster sets of each antenna are generated based on birth-death process on the array axis. The flowchart of the cluster generation algorithm is shown in Fig. 2.

First, let the initial number of clusters be N, the initial cluster set of Ant_1^T be $C_1^T = \{c_1^T, c_2^T, c_x^T, \cdots, c_N^T\}$, and the initial cluster set of Ant_1^R be $C_1^R = \{c_1^R, c_2^R, c_x^R, \cdots, c_N^R\}$, where c_x^T and c_x^R denote cluster members of cluster sets of the transmitter and the receiver, and the subscript $x(x = 1, 2, \cdots, N)$ of c_x^T and c_x^R denotes the cluster indices. The cluster sets of the rest of antennas at the transmitter side $C_l^T (l = 2, 3, \cdots, M_T)$ and the receiver side $C_k^R (k = 2, 3, \cdots, M_R)$ can be generated from the evolution of C_1^T and C_1^R, respectively. The survival probability of clusters to the next antenna is calculated according to (21) and (22). At the same time, new clusters are generated based on Poisson process with mean numbers as (23) and (24). These newly generated clusters are added to the cluster sets of corresponding antennas. Since each cluster evolves gradually on the antenna array, i.e., it will not appear again after its disappearance, antenna correlations have been naturally embedded in the generation process.

Second, after obtaining cluster sets of each antenna, $\bigcup_{l=1}^{M_T} C_l^T$ and $\bigcup_{k=1}^{M_R} C_k^R$ are the full collections of clusters observable to
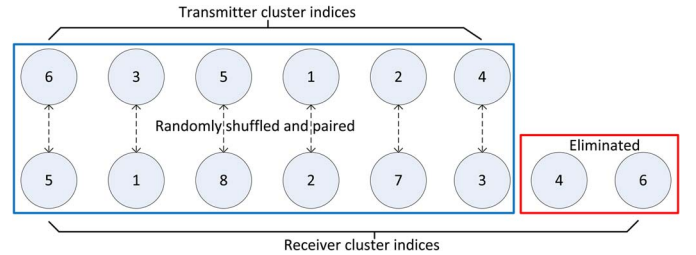

Fig. 3.   An example of random shuffling and pairing between the transmitter and receiver cluster indices.

the transmitter and receiver, respectively. To mimic the arbitrariness of the propagation environment, the cluster indices in $\bigcup_{l=1}^{M_T} C_l^T$ and $\bigcup_{k=1}^{M_R} C_k^R$ are shuffled and arranged in a random order. Then, cluster indices of the transmitter and receiver are paired. This process determines to which transmit and receive antennas each cluster is observable. An example of the random shuffling and pairing process has been illustrated in Fig. 3. In this example, transmit antennas who can observe c_6^T share a common cluster with receiver antennas who can observe c_5^R. Other clusters can be determined in the same way. Meanwhile, it is possible that the cardinalities of $\bigcup_{l=1}^{M_T} C_l^T$ and $\bigcup_{k=1}^{M_R} C_k^R$ are not equal, i.e., there are clusters that are not observable to either

the transmit array or the receive array. It can be seen in Fig. 3 that two more clusters are observable to the receiver than the transmitter. In this case, after random shuffling and pairing, two clusters are eliminated from the full receiver cluster set. Then, the cluster indices of these remained clusters are reassigned from 1 to N_{total}.

Last, the delays and mean power of clusters are generated according to the urban macro-cell scenario in [20] where delays and mean power are drawn randomly obeying the exponential distributions. After delays are obtained, the semi-major axes can be determined via (14). Since mean power is related to delay in [20], the mean power of a cluster is then related to the size of its corresponding ellipse. In addition, AoAs are modeled as the von Mises distribution [41]. As von Mises distribution can be easily adapted to other distributions such as uniform distribution and wrapped Gaussian distribution, it is widely utilized in the literature [8], [13], [14] to model angular dispersions.

B. Space Cross-Correlation Function (CCF) Analysis

Regarding the analysis of the spatial properties of the wideband model for massive MIMO with cluster evolution on the antenna arrays, the space CCF is introduced in this section. The normalized space CCF $\rho_{kl,k'l',n}(\delta_T, \delta_R; t)$ between the link connecting Ant_k^R and Ant_l^T and the link connecting $\text{Ant}_{k'}^R$ and $\text{Ant}_{l'}^T$ of the n-th cluster at time t is defined as [8], [42]

$$\rho_{kl,k'l',n}(\delta_T, \delta_R; t) = \mathrm{E}\left[\frac{h_{kl,n}(t)h_{k'l',n}^*(t)}{|h_{kl,n}(t)|\left|h_{k'l',n}^*(t)\right|} \right] \quad (25)$$

where $h_{k'l',n}^*(t)$ denotes the conjugate of $h_{k'l',n}(t)$. The LOS component and the NLOS components are independent to each other. As a result, the space CCF can be rewritten as the sum of the spatial correlation of the LOS component $\rho_{kl,k'l',n}^{\text{LOS}}(\delta_T, \delta_R; t)$ and the spatial correlation of the NLOS components $\rho_{kl,k'l',n}^{\text{NLOS}}(\delta_T, \delta_R; t)$.

$$\rho_{kl,k'l',n}(\delta_T, \delta_R; t) = \rho_{kl,k'l',n}^{\text{LOS}}(\delta_T, \delta_R; t) + \rho_{kl,k'l',n}^{\text{NLOS}}(\delta_T, \delta_R; t). \quad (26)$$

For the spatial correlation of the LOS component,

$$\rho_{kl,k'l',n}^{\text{LOS}}(\delta_T, \delta_R; t)$$
$$= \frac{K\delta(n-1)}{K+1} e^{j\left(2\pi f_{kl}^{\text{LOS}}t + \varphi_{kl}^{\text{LOS}} - 2\pi f_{k'l'}^{\text{LOS}}t - \varphi_{k'l'}^{\text{LOS}}\right)}. \quad (27)$$

For the spatial correlation of the NLOS components, a cluster observable to Ant_l^T and Ant_k^R has a probability of $e^{-\lambda_R|l-l'|\delta_T/D_c^a}e^{-\lambda_R|k-k'|\delta_R/D_c^a}$ to survive to connect $\text{Ant}_{l'}^T$ and $\text{Ant}_{k'}^R$. Since the number of rays is infinite in the theoretical model, the discrete AoAs $\alpha_{n,i}^R$ can be represented by a continuous random variable α_n^R. Therefore, given the probability density function (PDF) of the AoA $p_{\alpha_n^R}(\alpha_n^R)$, $\rho_{kl,k'l',n}^{\text{NLOS}}(\delta_T, \delta_R; t)$ can be computed as

$$\rho_{kl,k'l',n}^{\text{NLOS}}(\delta_T, \delta_R; t) = \frac{e^{\lambda_R \frac{-|l-l'|\delta_T - |k-k'|\delta_R}{D_c^a}}}{K\delta(n-1)+1}$$
$$\times \int_{-\pi}^{\pi} e^{j\left[\varphi_{kl,n}(\alpha_n^R) - \varphi_{k'l',n}(\alpha_n^R)\right]} p_{\alpha_n^R}(\alpha_n^R)\, d\alpha_n^R. \quad (28)$$
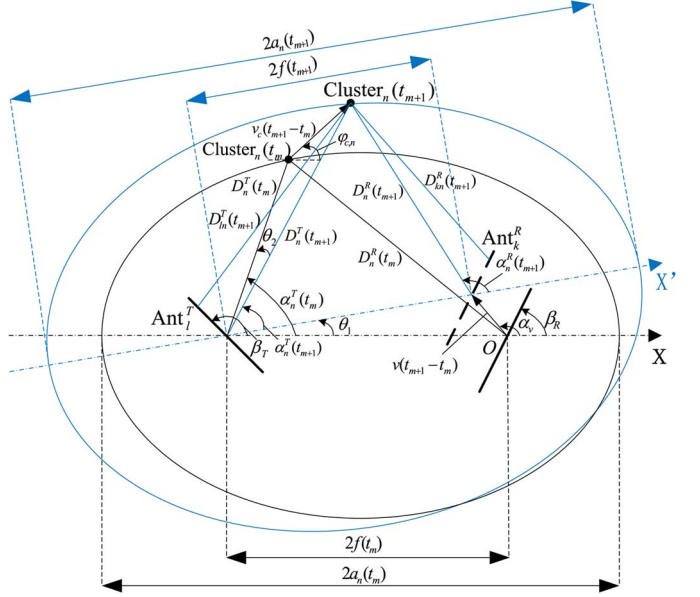

Fig. 4. Geometrical relationship evolution from $t = t_m$ to $t = t_{m+1}$ of the ellipse model.

Equations (27) and (28) indicate that the difference between $\varphi_{kl,n}$ and $\varphi_{k'l',n}$, $\varphi_{kl,n} - \varphi_{k'l',n}$ does not only depend on the difference between subscripts $l - l'$ and $k - k'$. This means the process on the array axis is not wide-sense stationary (WSS).

III. ARRAY-TIME EVOLUTION MODEL

To describe the cluster evolution on both array and time axes, the proposed wideband ellipse model is further improved by combining the birth-death process on the time axis in [33]. As a result, an array-time evolution model is established. Additionally, geometrical relationships among the transmitter, the receiver, and the clusters need to be updated with time. An example of a cluster evolving on time axis is illustrated in Fig. 4. Both clusters and the MS are moving. Cluster_n and the receive antenna array move to new positions from $t = t_m$ to $t = t_{m+1}$. Distances and angle properties have to be updated based on geometrical relationships. It can be seen that AoD, AoA, and transmission distance will be time-variant because of the movement of the cluster and the terminal. Consequently, α_n^T, α_n^R, D_n^T, D_n^R, D_{ln}^T, D_{kn}^R, a_n, f, α_v, and τ_n become time-variant as $\alpha_n^T(t)$, $\alpha_n^R(t)$, $D_n^T(t)$, $D_n^R(t)$, $D_{ln}^T(t)$, $D_{kn}^R(t)$, $a_n(t)$, $f(t)$, $\alpha_v(t)$, and $\tau_n(t)$ correspondingly. Although there exists situations when BS, MS, and clusters are all moving, it should be noticed that those situations can be equivalent to a static BS situation using the principles of relative motion.

In this case, assume Cluster_n, $(n = 1, 2, \cdots, N)$ moves in an arbitrary direction $\varphi_{c,n}$ with a speed of v_c at time instance $t = t_m(m = 1, 2, \cdots)$, then at $t = t_{m+1}$, the instant distance between two focal points $f(t_{m+1})$ can be calculated as

$$2f(t_{m+1}) = \Big[[2f(t_m)]^2 + [v(t_{m+1} - t_m)]^2$$
$$+ 4f(t_m)v(t_{m+1} - t_m)\cos[\alpha_v(t_m)] \Big]^{1/2}. \quad (29)$$

Accordingly, the distance between the transmitter and Cluster_n, $D_n^T(t)$, needs to be updated at $t = t_{m+1}$ as

$$D_n^T(t_{m+1}) = \Big[\big[D_n^T(t_m)\big]^2 + v_c^2(t_{m+1} - t_m)^2$$
$$+ 2D_n^T(t_m)v_c(t_{m+1} - t_m)\cos\big(\alpha_n^T(t_m) - \varphi_{c,n}\big)\Big]^{1/2}. \quad (30)$$

Referencing the instant ellipse of $\text{Cluster}_n(t_{m+1})$, the instant AoD and the distance between Ant_l^T and Cluster_n, $D_{ln}^T(t_{m+1})$ can be obtained as

$$\alpha_n^T(t_{m+1}) = \alpha_n^T(t_m) - \theta_1 - \theta_2 \quad (31)$$

$$\theta_1 = \arcsin\left[\frac{v(t_{m+1} - t_m)\sin(\pi - \alpha_v(t_m))}{2f(t_{m+1})}\right] \quad (32)$$

$$\theta_2 = \arcsin\left[\frac{v_{c,n}(t_{m+1} - t_m)\sin(\pi - \alpha_n^T(t_m) + \varphi_{c,n})}{D_n^T(t_{m+1})}\right] \quad (33)$$

$$D_{ln}^T(t_{m+1}) = \Bigg[D_n^T(t_{m+1})^2 + \left(\frac{M_T - 2l + 1}{2}\delta_T\right)^2$$
$$- D_n^T(t_{m+1})(M_T - 2l + 1)\delta_T \cos\big(\beta_T - \alpha_n^T(t_{m+1})\big)\Bigg]^{1/2}. \quad (34)$$

Similarly, the distance between the receiver and Cluster_n, $D_n^R(t)$, the corresponding instant delay $\tau_n(t_{m+1})$, and the instant movement direction $\alpha_v(t_{m+1})$ of the receiver are derived as

$$D_n^R(t_{m+1}) = \Big[[2f(t_{m+1})]^2 + \big[D_n^T(t_{m+1})\big]^2$$
$$- 4f(t_{m+1})D_n^T(t_{m+1})\cos\big(\alpha_n^T(t_{m+1})\big)\Big]^{1/2} \quad (35)$$

$$2a_n(t_{m+1}) = D_n^T(t_{m+1}) + D_n^R(t_{m+1}) \quad (36)$$

$$\tau_n(t_{m+1}) = \tau_n(t_m) + \frac{2a_n(t_{m+1}) - 2a_n(t_m)}{c} \quad (37)$$

$$\alpha_v(t_{m+1}) = \alpha_v(t_m) - \theta_1. \quad (38)$$

Next, according to the law of sines, the AoA of Cluster_n at $t = t_{m+1}$, the distance between Ant_k^R and Cluster_n, $D_{kn}^R(t_{m+1})$, and Doppler frequency $f_n(\alpha_n^R(t_{m+1}))$ are computed as

$$\alpha_n^R(t_{m+1}) = \arcsin\left[\frac{D_n^T(t_{m+1})\sin\big[\alpha_n^T(t_{m+1})\big]}{D_n^R(t_{m+1})}\right] \quad (39)$$

$$D_{kn}^R(t_{m+1}) = \Bigg[D_n^R(t_{m+1})^2 + \left(\frac{M_R - 2k + 1}{2}\delta_R\right)^2$$
$$- D_n^R(t_{m+1})(M_R - 2k + 1)\delta_R \cos\big(\alpha_n^R(t_{m+1}) - \beta_R + \theta_1\big)\Bigg]^{1/2} \quad (40)$$

$$f_n\big(\alpha_n^R(t_{m+1})\big) = f_{\max}\cos\big(\alpha_n^R(t_{m+1}) - \alpha_v(t_{m+1})\big). \quad (41)$$

Besides geometrical relationships, cluster sets of each antenna evolve with time as well. Thus, the time-variant C_l^T, C_k^R, and N_{new} are denoted as $C_l^T(t)$, $C_k^R(t)$, and $N_{\text{new}}(t)$, respectively. The evolution of clusters on the time axis is modeled as a birth-death process [33]. Here, let $C_l^T(t_m)(l = 1, 2, \cdots, M_T; m = 0, 1, 2, \cdots)$ and $C_k^R(t_m)(k = 1, 2, \cdots, M_R; m = 0, 1, 2, \cdots)$ denote the cluster set for Ant_l^T and the cluster set for Ant_k^R at time instant t_m. Then at the next time instant, each cluster

member in set $\{(\bigcup_{l=1}^{M_T} C_l^T(t_m)) \bigcup (\bigcup_{k=1}^{M_R} C_k^R(t_m))\}$ evolves according to the birth-death process on the time axis. A survived cluster member will remain in cluster sets. On the other hand, a disappeared cluster member will be eliminated from all the cluster sets. Newly generated cluster members will be added to certain cluster sets according to the birth-death process on the array axis. To sum up, the algorithm is based on two main operations, the array-axis evolution and the time-axis evolution, an example is described as follows.

At the initial time instant $t = t_m$, array-axis evolution will be first operated. As Fig. 2 indicates, given $C_1^T(t_m)$ and $C_1^R(t_m)$, the cluster set of Ant_l^T is evolved from the cluster set of Ant_{l-1}^T, the cluster set of Ant_k^R is evolved from the cluster set of Ant_{k-1}^R

$$C_{l-1}^T(t_m) \xrightarrow{\text{E}} C_l^T(t_m) \quad 2 \le l \le M_T \quad (42)$$

$$C_{k-1}^R(t_m) \xrightarrow{\text{E}} C_k^R(t_m) \quad 2 \le k \le M_R. \quad (43)$$

Then, at the next time instant $t = t_{m+1}$, time-axis evolution is operated as proposed in [33]

$$C_l^T(t_m) \xrightarrow{\text{E}} C_l^T(t_{m+1}) \quad (44)$$

$$C_k^R(t_m) \xrightarrow{\text{E}} C_k^R(t_{m+1}). \quad (45)$$

To perform the evolution process of clusters on the time axis as (44) and (45) show, define channel fluctuation in time domain at $t = t_{m+1}$ as q_{m+1}. The channel fluctuation is a measure of how much the scattering environment has changed. Assuming that the receiver and clusters are moving with a constant velocity, q_{m+1} is defined as [33]

$$q_{m+1} = q_{x,m+1} + q_{t,m+1} \quad (46)$$

where $q_{x,m+1}$ is the fluctuation caused by the movement of receiver [33]

$$q_{x,m+1} = v(t_{m+1} - t_m) \quad (47)$$

and $q_{t,m+1}$ is the fluctuation caused by the movement of clusters (P_F is the percentage of moving clusters, v_c is the velocity of clusters) [33]

$$q_{t,m+1} = P_F v_c(t_{m+1} - t_m). \quad (48)$$

Given the scenario-dependent correlation factor D_c^s on the space axis, each cluster survives with probability P_{survival}, which can be calculated as [45]

$$P_{\text{survival}}(q_{m+1}) = e^{-\frac{\lambda_R q_{m+1}}{D_c^s}}. \quad (49)$$

New clusters are generated according the Poisson process. The mean number of newly generated clusters at time instant $t = t_{m+1}$ on the time axis $\text{E}[N_{\text{new}}(t_{m+1})]$ is presented as [45]

$$\text{E}[N_{\text{new}}(t_{m+1})] = \frac{\lambda_G}{\lambda_R}\left(1 - e^{-\frac{\lambda_R q_{m+1}}{D_c^s}}\right). \quad (50)$$

For survived clusters, their geometrical relationships are computed as from (29) to (41). On the other hand, the delays, mean

power of newly generated clusters are randomly drawn according to [20], where delays and mean power are exponentially distributed. The AoAs of newly generated clusters obey the von Mises distribution. To decide which transmit (receive) antennas are able to observe a newly generated cluster, the newly generated cluster is first attached to one transmit (receive) antenna with a randomly drawn index, say the ν-th transmit (receive) antenna. Second, this cluster evolves to both ends of the transmit (receive) antenna array, $\nu + 1$ to M_T and $\nu - 1$ to 1 (or $\nu + 1$ to M_R and $\nu - 1$ to 1), based on the survival probabilities on the array axis $P_{\text{survival}}^T (P_{\text{survival}}^R)$. Third, this cluster is added to antenna cluster sets if it survives on those corresponding antennas. Finally, all cluster sets $C_l^T(t_{m+1})$ and $C_k^R(t_{m+1})$ have been updated before entering the next time instant.

Prior to the derivation of STFCF, the time-variant transfer function $H_{kl}(\xi, t)$ of the channel can be expressed as [8]

$$H_{kl}(\xi, t) = \int_{-\infty}^{\infty} h_{kl}(t, \tau) e^{-j2\pi\xi\tau} d\tau$$

$$= \int_{-\infty}^{\infty} \sum_{n=1}^{N_{\text{total}}} h_{kl,n}(t) \delta(\tau - \tau_n) e^{-j2\pi\xi\tau} d\tau$$

$$= \sum_{n=1}^{N_{\text{total}}} h_{kl,n}(t) e^{-j2\pi\xi\tau_n} \tag{51}$$

where ξ is frequency. The normalized STFCF $\rho_{kl,k'l'}(\delta_T, \delta_R, \Delta\xi, \Delta t; \xi, t)$ can be calculated as [8]

$$\rho_{kl,k'l'}(\delta_T, \delta_R, \Delta\xi, \Delta t; \xi, t)$$

$$= \mathrm{E}\left[\frac{H_{kl}^*(\xi, t) H_{k'l'}(\xi + \Delta\xi, t + \Delta t)}{|H_{kl}^*(\xi, t)| \, |H_{k'l'}(\xi + \Delta\xi, t + \Delta t)|} \right]$$

$$= \mathrm{E}\left[\frac{\sum_{m=1}^{N_{\text{total}}} \sum_{n=1}^{N_{\text{total}}} h_{kl,m}^*(t) h_{k'l',n}(t + \Delta t) e^{j2\pi\xi\tau_m - j2\pi(\xi + \Delta\xi)\tau_n}}{|H_{kl}^*(\xi, t)| |H_{k'l'}(\xi + \Delta\xi, t + \Delta t)|} \right]. \tag{52}$$

With the uncorrelated scattering (US) assumption, i.e., clusters are mutually independent

$$\mathrm{E}\left[h_{kl,m}^*(t) h_{k'l',n}(t + \Delta t) \right] = 0 \tag{53}$$

for $m \neq n$, the STFCF in (52) reduces to

$$\rho_{kl,k'l'}(\delta_T, \delta_R, \Delta\xi, \Delta t; t)$$

$$= \mathrm{E}\left[\frac{\sum_{n=1}^{N_{\text{total}}} h_{kl,n}^*(t) h_{k'l',n}(t + \Delta t) e^{j2\pi\Delta\xi\tau_n}}{|H_{kl}^*(\xi, t)| \, |H_{k'l'}(\xi + \Delta\xi, t + \Delta t)|} \right]$$

$$= \mathrm{E}\left[\frac{\sum_{n=1}^{N_{\text{total}}} h_{kl,n}^*(t) h_{k'l',n}(t + \Delta t) e^{j2\pi\Delta\xi\tau_n}}{|H_{kl}^*(\xi, t)| \, |H_{k'l'}(\xi + \Delta\xi, t + \Delta t)|} \right]$$

$$= \sum_{n=1}^{N_{\text{total}}} w_n \rho_{kl,k'l',n}(\delta_T, \delta_R, \Delta\xi, \Delta t; t) \tag{54}$$

where $\{w_n\}$ are normalization weights such that $\sum_{n=1}^{N_{\text{total}}} w_n \rho_{kl,k'l',n}(0,0,0,0; t) = 1$ and the normalized STFCF for the n-th cluster $\rho_{kl,k'l',n}(\delta_T, \delta_R, \Delta\xi, \Delta t; t)$ is defined by

$$\rho_{kl,k'l',n}(\delta_T, \delta_R, \Delta\xi, \Delta t; t)$$

$$= \mathrm{E}\left[\frac{h_{kl,n}^*(t) h_{k'l',n}(t + \Delta t) e^{j2\pi\Delta\xi\tau_n}}{\left| h_{kl,n}^*(t) \right| \left| h_{k'l',n}(t + \Delta t) \right|} \right]. \tag{55}$$

By setting $l = l'$, $k = k'$, and $\Delta\xi = 0$, since a cluster has a probability of $e^{-\lambda_R \frac{v\Delta t + P_F v_c \Delta t}{D_c^s}}$ to survive from t to $t + \Delta t$, the time autocorrelation function (ACF) of the wideband ellipse massive MIMO of the n-th cluster with considerations on cluster evolution on the time axis, $\rho_{kl,n}(\Delta t; t)$, can be computed as

$$\rho_{kl,n}(\Delta t; t) = \rho_{kl,k'l',n}(0, 0, 0, \Delta t; t)$$

$$= \mathrm{E}\left[\frac{h_{kl,n}^*(t) h_{kl,n}(t + \Delta t)}{\left| h_{kl,n}^*(t) \right| \left| h_{kl,n}(t + \Delta t) \right|} \right]$$

$$= e^{-\lambda_R \frac{v\Delta t + P_F v_c \Delta t}{D_c^s}}$$

$$\times \int_{-\pi}^{\pi} e^{j\left[2\pi f_n(\alpha_n^R(t + \Delta t))(t + \Delta t) - 2\pi f_n(\alpha_n^R(t))t + \varphi_{kl,n}(t + \Delta t) - \varphi_{kl,n}(t) \right]}$$

$$\times p_{\alpha_n^R}(\alpha_n^R) \, d\alpha_n^R \tag{56}$$

where $\varphi_{kl,n}(t)$ and $f_n(\alpha_n^R(t))$ can be respectively calculated as given by (19) and (20) including time variations. As can be seen in (56), the time correlation function is time t dependent, hence the model is not WSS on the time axis.

By setting $l = l'$, $k = k'$, and $\Delta t = 0$, the STFCF in (52) reduces to the frequency correlation function (FCF) $\rho_{kl}(\Delta\xi; t)$

$$\rho_{kl}(\Delta\xi; t) = \rho_{kl,k'l'}(0, 0, \Delta\xi, 0; t)$$

$$= \mathrm{E}\left[\frac{\sum_{n=1}^{N_{\text{total}}} h_{kl,n}^*(t) h_{k'l',n}(t) e^{j2\pi\Delta\xi\tau_n}}{|H_{kl}^*(\xi, t)| \, |H_{k'l'}(\xi + \Delta\xi, t)|} \right]$$

$$= \mathrm{E}\left[\frac{\sum_{n=1}^{N_{\text{total}}} |h_{kl,n}(t)|^2 e^{j2\pi\Delta\xi\tau_n}}{|H_{kl}^*(\xi, t)| \, |H_{kl}(\xi + \Delta\xi, t)|} \right]. \tag{57}$$
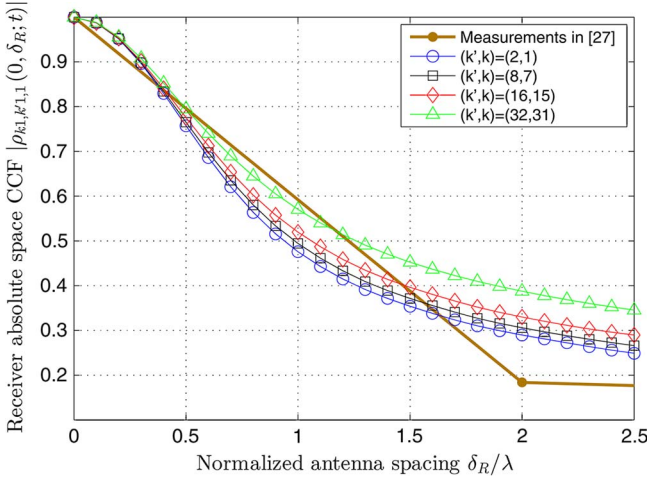
Fig. 5. Absolute receiver space CCF $|\rho_{k1,k'1,1}(0,\delta_R;t)|$ of the ellipse model under von Mises assumption in terms of different values of (k', k) pairs with $|k' - k| = 1$. ($M_R = 32$, $M_T = 1$, $t = 1$ s, $a_1 = 100$ m, $f = 80$ m, $D_c^a = 30$ m, $D_c^s = 50$ m, $\beta_R = \beta_T = \pi/2$, $\lambda = 0.12$ m, $f_{\max} = 33.33$ Hz, $\alpha_v = \pi/6$, $\kappa = 5$, $\bar{\alpha}_n^R = \pi/3$, NLOS).

IV. NUMERICAL ANALYSIS

In this section, numerical results of the proposed model will be analyzed. To perform numerical analysis, delays and mean power of clusters are assumed to be generated according to the urban macro-cell scenario in [20] where both of them follow the exponential distributions. AoAs of clusters to the receive array center are assumed to be von Mises distributed. The von Mises distribution can be characterized by its PDF [43]

$$p_{\alpha_n^R}\left(\alpha_n^R\right) = \frac{\exp\left[\kappa\cos\left(\alpha_n^R - \bar{\alpha}_n^R\right)\right]}{2\pi I_0(\kappa)} \quad \alpha_n^R \in [-\pi, \pi] \quad (58)$$

where $I_0(\cdot)$ is the zero-th order modified Bessel function, $\bar{\alpha}_n^R$ is the mean and $\kappa \geq 0$ controls the width of the distribution.

The receiver absolute space CCF $|\rho_{k1,k'1,1}(0,\delta_R;t)|$ of the ellipse model under spherical assumption in terms of different values of (k', k) pairs with $|k' - k| = 1$ is illustrated in Fig. 5. It can be observed that the receive antenna correlation slowly decreases as the normalized antenna spacing increases. The numerical results of the receive antenna correlation curves of the proposed model are compared with measurements on receiver correlation of massive MIMO in [27], showing that they share a similar trend. Most importantly, it can be realized that correlation functions of different values of k' and k with $|k' - k| = 1$ are different. The correlation function does not only depend of the absolute difference between antenna indices but also the indices of reference antennas, which means the WSS properties on the antenna array axis are not valid under the spherical wavefront assumption. The absolute space CCF $|\rho_{11,22,1}(\delta_T, \delta_R;t)|$ of the ellipse model under spherical assumption has been illustrated in Fig. 6. It can be observed that the spatial correlation gradually drops when the normalized antenna spacing increases.

Furthermore, an example of cluster evolution on the array axis has been depicted in Fig. 7. Originally there are 20 clusters (Cluster$_1$ to Cluster$_{20}$) observable to the first antenna element. Then, these clusters evolve according to the birth-death process

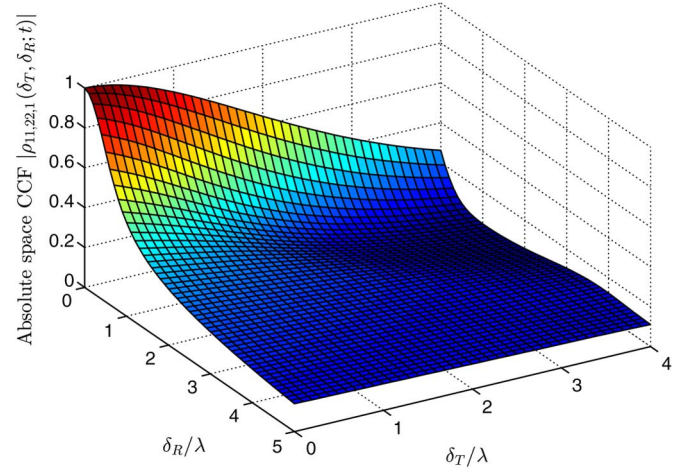

Fig. 6. Absolute space CCF $|\rho_{11,22,1}(\delta_T, \delta_R;t)|$ of the ellipse model. ($M_R = M_T = 32$, $t = 1$ s, $a_1 = 100$ m, $f = 80$ m, $D_c^a = 30$ m, $D_c^s = 50$ m, $\beta_R = \beta_T = \pi/2$, $\lambda = 0.15$ m, $f_{\max} = 33.33$ Hz, $\alpha_v = \pi/6$, $\kappa = 5$, NLOS).
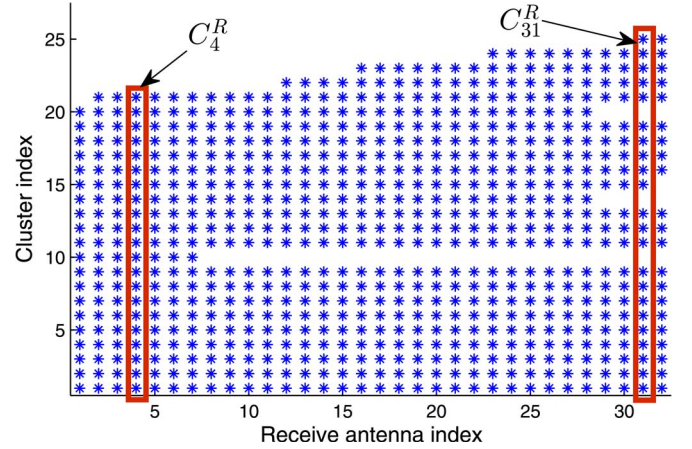

Fig. 7. An example of cluster evolution on the receive antenna array. (A "$*$" symbol in the two dimensional plane means its corresponding antenna element (coordinate on the horizontal direction) is able to observe its corresponding cluster (coordinate on the vertical direction).)

and probabilities described in Section II-A. It can be observed that 4 (Cluster$_{10}$, Cluster$_{14}$, Cluster$_{15}$, and Cluster$_{20}$) of the original 20 clusters disappear during the evolutin process and 5 new clusters (Cluster$_{21}$ to Cluster$_{25}$) have been generated. As a result, different antenna elements may observe different cluster sets. The cluster sets of the 4th and the 31st receive antennas C_4^R and C_{31}^R, for instance, share 18 common clusters. It should be noticed that, unlike conventional MIMO channel models, only a total cluster number of a cluster set is not sufficient to represent the properties of the cluster. The cluster members inside a cluster set as well as their properties such as delay, AoA and cluster power should be considered when calculating the channel coefficients in (3).

Figs. 8 and 9 show the normalized angle power spectrum (APS) of AoA of the wideband ellipse model for both NLOS and LOS scenarios. The value of λ_R is set as 4/m, the values of λ_G are chosen as 80/m and 32/m for NLOS and LOS cases, respectively. Hence, the mean numbers of clusters are aligned with NLOS (20 clusters) and LOS (8 clusters) cases in the
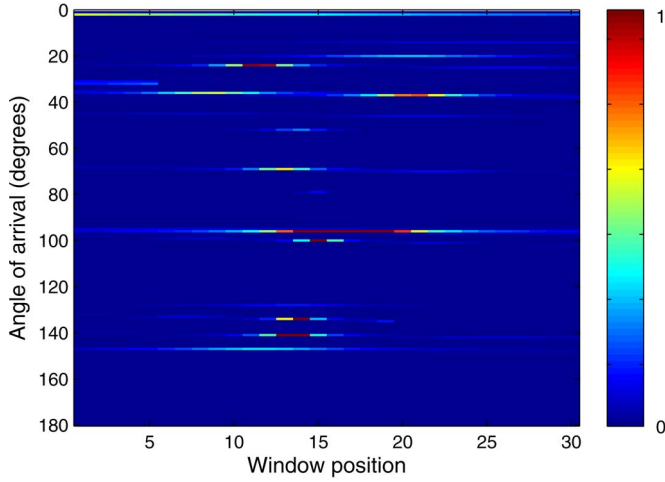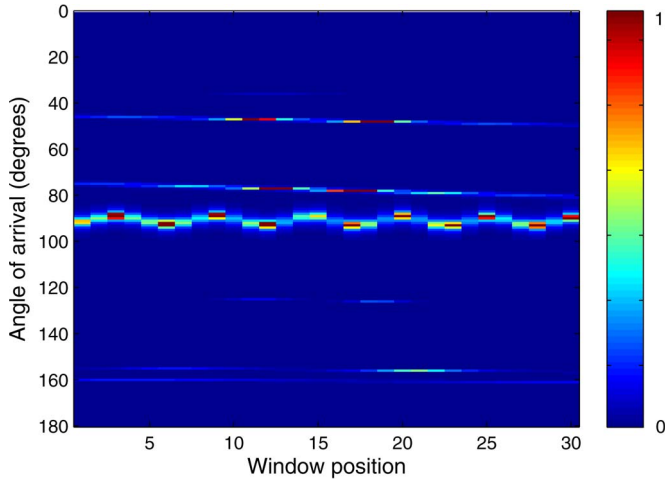
Fig. 8. A snapshot example of the normalized angle power spectrum of AoA of the wideband ellipse model. ($M_R = 32$, $M_T = 1$, $a_1 = 100$ m, $f = 80$ m, $D_c^a = 30$ m, $D_c^s = 50$ m, $\beta_R = \beta_T = \pi/2$, $\lambda = 0.15$ m, $\delta_R = 0.5\lambda$, $f_{\max} = 0$ Hz, NLOS, $\lambda_G = 80/\text{m}$, $\lambda_R = 4/\text{m}$, $P_F = 0.3$).

Fig. 9. A snapshot example of the normalized angle power spectrum of AoA of the wideband ellipse model. ($M_R = 32$, $M_T = 1$, $a_1 = 100$ m, $f = 80$ m, $D_c^a = 30$ m, $D_c^s = 50$ m, $\beta_R = \beta_T = \pi/2$, $\lambda = 0.15$ m, $\delta_R = 0.5\lambda$, $f_{\max} = 0$ Hz, LOS $K = 3$ dB, $\lambda_G = 32/\text{m}$, $\lambda_R = 4/\text{m}$, $P_F = 0.3$).

WINNER II model. The AoAs are estimated using the well-known multiple signal classification (MUSIC) algorithm [46], [47] with a sliding window formed by 3 consecutive antennas. This sliding window is shifted by 1 antenna at a time, from the first antenna to the last antenna. Therefore, for a 32-element antenna array, there are in total 30 window positions as Figs. 8 and 9 illustrate. Three properties can be observed via these two figures. First, it can be observed that several estimated AoAs gradually change along the array axis. This phenomenon is mainly caused by the spherical wavefront assumption when the distances between their corresponding clusters and the antenna array do not fulfill the farfield assumption. Consequently, the AoAs of these clusters are no longer constant on every antenna element. Second, it is the birth-death process that models the dynamic properties of clusters and the non-stationarities on the array axis, where the appearance and disappearance of clusters can be seen in both figures. Different antenna elements may
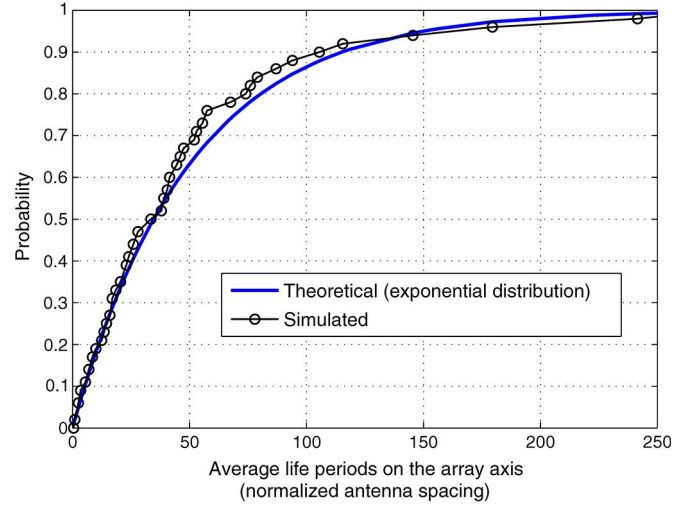

Fig. 10. Cumulative distribution function of average life periods of clusters on the array axis in terms of normalized antenna spacing. ($D_c^a = 30$ m, $D_c^s = 50$ m, $\lambda = 0.15$ m, $\delta_R = 0.5\lambda$, NLOS, $\lambda_G = 80/\text{m}$, $\lambda_R = 4/\text{m}$, $P_F = 0.3$).

observe different sets of clusters, and the life periods of these clusters are continuous on the array axis.

The CDF of the average life periods of clusters on the array axis is illustrated in Fig. 10. It shows the survival probability of a cluster decreases exponentially as evolving on the array axis. Third, the power variations of each cluster result in imbalanced received power on the array axis. To study this phenomenon, let $p_k (k = 1, \cdots, M_R)$ denote the received power of Ant_k^R, then the maximum received power difference $\Delta p_{\max}^R$ is defined as

$$\Delta p_{\max}^R (\text{dB}) = 10 \log_{10} \frac{\max\{p_1, p_2, \cdots, p_{M_R}\}}{\min\{p_1, p_2, \cdots, p_{M_R}\}}. \quad (59)$$

After 200 trials, the CDF of the the maximum received power difference in difference conditions of correlation factors on array and space axes can be observed in Fig. 11. It shows a difference of approximately 2–3 dB between the maximum and minimum received power over the antenna array, which is normally not investigated in conventional plane wavefront MIMO channel models. Also, the received power difference on the array axis increases as the correlation factor reduces. Similar conclusions on received power imbalance can be found in [27] and [28].

The absolute receiver space CCFs of the wideband ellipse model with different birth-death process configurations is illustrated in Fig. 12. It can be observed that the correlation with cluster evolution on the array axis is lower than that without considering array evolution, because a certain number of clusters would fail to survive when they evolve on the array axis. Also, the gap between the two curves increases as the antenna separation grows because of a lower probability for a cluster to survive. Finally, the time-variant characteristic has been shown in Fig. 13. It can be observed that the absolute time ACF varies along with time and hence the numerical result demonstrates time non-stationarities of the model.

Fig. 14 compares the FCF between NLOS and LOS scenarios. It can be seen that the FCF of NLOS decreases significantly with the frequency difference whose 50% coherence bandwidth is approximately 1.2 MHz. On the other hand, the LOS scenario
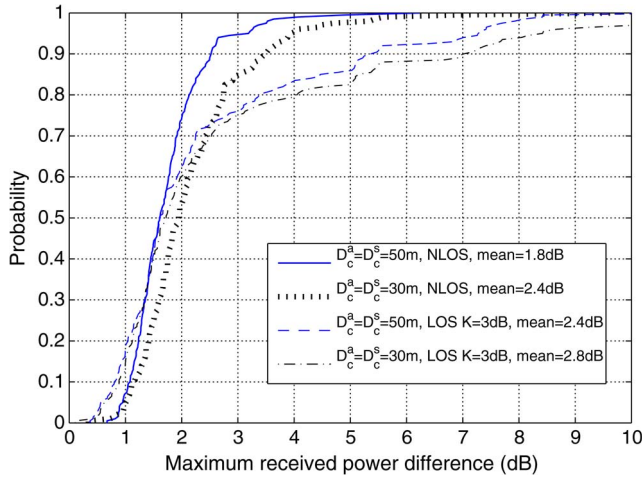
Fig. 11. Cumulative distribution function of the maximum power difference over the antenna array under different LOS/NLOS conditions and correlation factors on array and space axes. ($M_R = 32$, $M_T = 1$, $a_1 = 100$ m, $f = 80$ m, $\beta_R = \beta_T = \pi/2$, $\lambda = 0.15$ m, $\delta_R = 0.5\lambda$, $f_{\max} = 0$ Hz, von Mises distributed AoA).
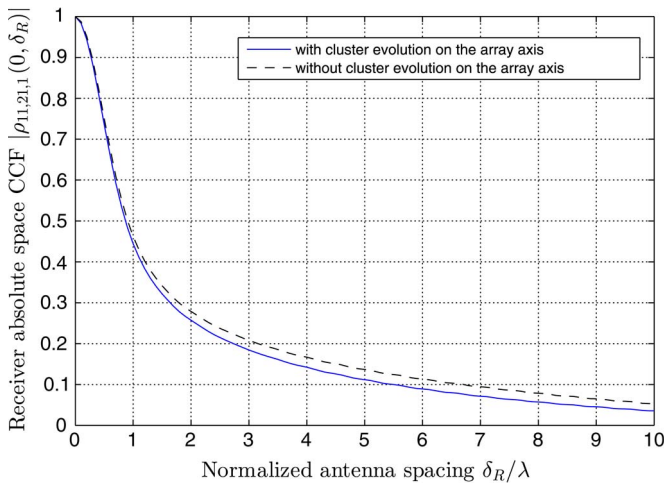

Fig. 12. Absolute receiver space CCF $|\rho_{11,21,1}(0, \delta_R; t)|$ of the wideband ellipse model. ($M_R = 32$, $M_T = 1$, $t = 1$ s, $a_1 = 100$ m, $f = 80$ m, $D_c^a = 15$ m, $D_c^s = 50$ m, $\beta_R = \beta_T = \pi/2$, $\lambda = 0.15$ m, $\delta_R = 0.5\lambda$, $f_{\max} = 0$ Hz, NLOS, $\lambda_G = 80$/m, $\lambda_R = 4$/m, $P_F = 0.3$, $\kappa = 5$).

has a larger 50% coherence bandwidth because the LOS component dominates the power of the channel.

V. CONCLUSION

A novel 2D wideband ellipse channel model with non-stationarities on both time and array axes for massive MIMO communication systems has been proposed in this paper. Spherical wavefront has been assumed in the proposed model illustrating the difference of spatial correlation properties compared with the plane wavefront assumption used in conventional MIMO channel models. It has been demonstrated that WSS properties are not available under the spherical wavefront assumption. Additionally, birth-death process has been applied to both time and array axes to model the non-stationary behaviors of clusters on both axes. In this case, different cluster sets can be observable to different antenna elements in this model. Finally,
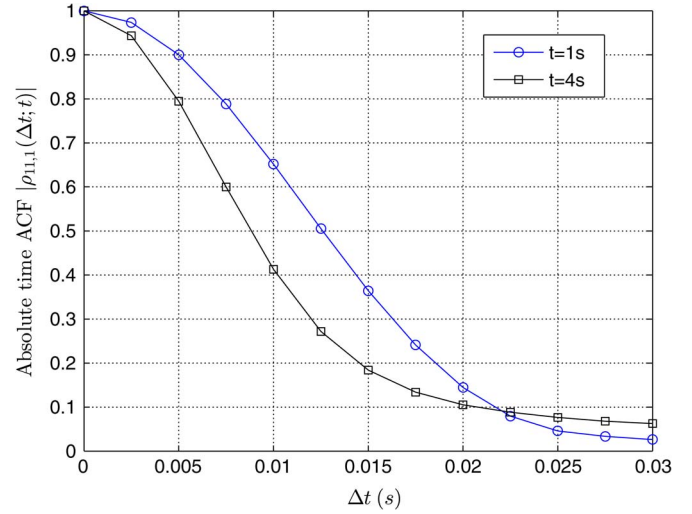

Fig. 13. Absolute time ACF of Cluster$_1$ $|\rho_{11,1}(\Delta t; t)|$ in (56) comparison between $t = 1$ s and $t = 4$ s with birth-death process. ($M_R = 32$, $M_T = 32$, $a_1 = 100$ m, $f = 80$ m, $D_c^a = 15$ m, $D_c^s = 50$ m, $\beta_R = \beta_T = \pi/2$, $\lambda = 0.15$ m, $\delta_R = \delta_T = 0.5\lambda$, $f_{\max} = 33.33$ Hz, $v_c = 0.5$ m/s, NLOS, $\lambda_G = 80$/m, $\lambda_R = 4$/m, $P_F = 0.3$, $\kappa = 5$).

Fig. 14. Absolute FCF $|\rho_{11}(\Delta\xi; t)|$ comparison between NLOS and LOS. ($M_R = 32$, $M_T = 32$, $a_1 = 100$ m, $f = 80$ m, $D_c^a = 15$ m, $D_c^s = 50$ m, $\beta_R = \beta_T = \pi/2$, $\lambda = 0.15$ m, $\delta_R = \delta_T = 0.5\lambda$, $f_{\max} = 33.33$ Hz, $v_c = 0.5$ m/s, $\lambda_G = 80$/m, $\lambda_R = 4$/m, $P_F = 0.3$, $\kappa = 5$.
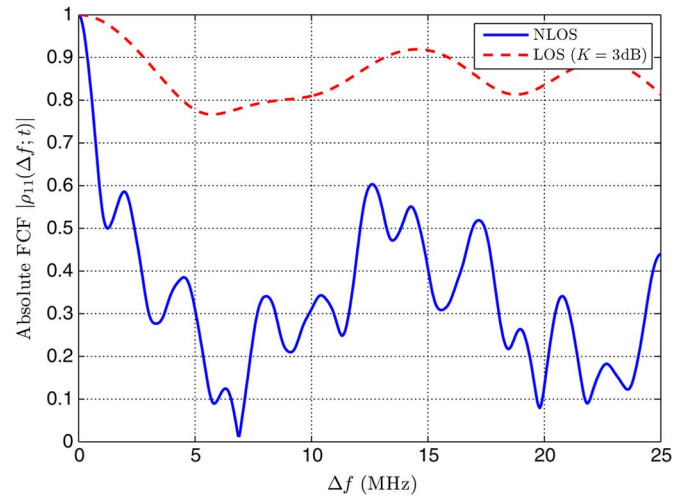
based on the numerical analysis, the proposed model has shown that there are non-stationarities and dynamic properties of clusters on the antenna array in massive MIMO channels, where similar conclusions have also been drawn in measurements [27] and [28]. For future work, certain parameters of the proposed channel model may be extracted via measurements. Also, since GBSMs do not depend on configurations of antenna arrays, polarized antenna arrays can be employed in future extensions of the channel model.

REFERENCES

[1] A. Paulraj, R. Nabar, and D. Gore, *Introduction to Space-Time Wireless Communications.*. Cambridge, U.K.: Cambridge Univ. Press, 2008.
[2] *IEEE 802.16 WG, 802.16m Evaluation Methodology Document*, 802.16m-08/004r5, Jan. 1999.
[3] "Physical Channels and Modulation," Sophia Antipolis Cedex, France, 3GPP T.S. 36.211 - V12.1.0, 2014.

[4] E. G. Larsson, F. Tufvesson, O. Edfors, and T. L. Marzetta, "Massive MIMO for next generation wireless systems," *IEEE Commun. Mag.*, vol. 52, no. 2, pp. 186–195, Feb. 2014.

[5] F. Rusek *et al.*, "Scaling up MIMO: Opportunities and challenges with very large arrays," *IEEE Signal Process. Mag.*, vol. 30, no. 1, pp. 40–60, Jan. 2012.

[6] K. Zheng, S. Ou, and X. Yin, "Massive MIMO channel models: A survey," *Hindawi Int. J. Antennas Propag.*, vol. 2014, pp. 848071-1–848071-10, Jun. 2014.

[7] L. Lu, G. Y. Li, A. L. Swindlehurst, A. Ashikhmin, and R. Zhang, "An overview of massive MIMO benefits and challenges," *IEEE J. Sel. Signal Process.*, vol. 8, no. 5, pp. 742–758, Oct. 2014.

[8] M. Patzold, *Mobile Radio Channels*, 2nd ed. West Sussex, England: Wiley, 2012.

[9] A. Ghazal, C.-X. Wang, B. Ai, D. Yuan, and H. Haas, "A non-stationary wideband MIMO channel model for high-mobility intelligent transportation systems," *IEEE Trans. Intell. Transp. Syst.*, vol. 16, no. 1, Feb. 2015.

[10] C.-X. Wang *et al.*, "Cooperative MIMO channel models: A survey," *IEEE Commun. Mag.*, vol. 48, no. 2, pp. 80–87, Feb. 2010.

[11] R. B. Ertel, P. Cardieri, K. W. Sowerby, T. S. Rappaport, and J. H. Reed, "Overview of spatial channel models for antenna array communication systems," *IEEE Pers. Commun.*, vol. 5, no. 1, pp. 10–22, Feb. 1998.

[12] J. C. Liberti and T. S. Rappaport, "A geometrically based model for line-of-sight multipath radio channels," in *Proc. IEEE VTC*, Atlanta, GA, USA, Apr. 1996, pp. 844–848.

[13] X. Cheng, C.-X. Wang, D. I. Laurenson, S. Salous, and A. V. Vasilakos, "An adaptive geometry-based stochastic model for non-isotropic MIMO mobile-to-mobile channels," *IEEE Trans. Wireless Commun.*, vol. 8, no. 9, pp. 4824–4835, Sep. 2009.

[14] X. Cheng, C.-X. Wang, B. Ai, and H. Aggoune, "Envelope level crossing rate and average fade duration of non-isotropic vehicle-to-vehicle Ricean fading channels," *IEEE Trans. Intell. Transp. Syst.*, vol. 15, no. 1, pp. 62–72, Feb. 2014.

[15] X. Cheng *et al.*, "Cooperative MIMO channel modeling and multi-link spatial correlation properties," *IEEE J. Sel. Areas Commun.*, vol. 30, no. 2, pp. 388–396, Feb. 2012.

[16] Y. Yuan, C.-X. Wang, X. Cheng, B. Ai, and D. I. Laurenson, "Novel 3D geometry-based stochastic models for non-isotropic MIMO vehicle-to-vehicle channels," *IEEE Trans. Wireless Commun.*, vol. 13, no. 1, pp. 298–309, Jan. 2014.

[17] A. G. Zajic, G. L. Stuber, T. G. Pratt, and S. T. Nguyen, "Wideband MIMO mobile-to-mobile channels: Geometry-based statistical modeling with experimental verification," *IEEE Trans. Veh. Technol.*, vol. 58, no. 2, pp. 517–534, Feb. 2009.

[18] H. Hofstetter, A. F. Molisch, and N. Czink, "A twin-cluster MIMO channel model," in *Proc. IEEE EuCAP*, Nice, France, Nov. 2006, pp. 1–8.

[19] C.-X. Wang, X. Hong, H. Wu, and W. Xu, "Spatial temporal correlation properties of the 3GPP spatial channel model and the Kronecker MIMO channel model," *EURASIP J. Wireless Commun. Netw.*, vol. 2007, pp. 39871-1–39871-9, 2007.

[20] P. Kyosti *et al.*, "WINNER II Channel Models," WINNER, Munich, Germany, D1.1.2 V1.1, Sep. 2007.

[21] "Guidelines for Evaluation of Radio Interface Technologies for IMT-Advanced," ITU, Geneva, 1211, Rep. ITU-R M.2135-1, 2009.

[22] N. Czink and C. Oestges, "The COST 273 MIMO channel model: Three kinds of clusters," in *Proc. ISSSTA*, Bologna, Italy, Aug. 2008, pp. 282–286.

[23] L. Liu *et al.*, "The COST 2100 MIMO channel model," *IEEE Commun. Mag.*, vol. 19, no. 6, pp. 92–99, Dec. 2012.

[24] R. Verdone and A. Zanella, *Pervasive Mobile and Ambient Wireless Communications: COST Action 2100*. London, U.K.: Springer-Verlag, 2012.

[25] C. K. Wen, S. Jin, and K. K. Wong, "On the sum-rate of multiuser MIMO uplink channels with jointly-correlated Rician fading," *IEEE Trans. Commun.*, vol. 59, no. 10, pp. 2883–2895, Oct. 2011.

[26] R. Couillet, M. Debbah, and J. Silverstein, "A deterministic equivalent for the capacity analysis of correlated multi-user MIMO channels," *IEEE Trans. Inf. Theory*, vol. 57, no. 6, pp. 3493–3514, Jun. 2011.

[27] S. Payami and F. Tufvesson, "Channel measurements and analysis for very large array systems at 2.6 GHz," in *Proc. 6th Eur. Conf. Antennas Propag.*, Prague, Czech Republic, Mar. 2012, pp. 433–437.

[28] X. Gao, F. Tufvesson, O. Edfors, and F. Rusek, "Measured propagation characteristics for very-large MIMO at 2.6 GHz," in *Proc. 46th Annu. Asilomar Conf. Signals, Syst., Comput.*, Pacific Grove, CA, USA, Nov. 2012, pp. 295–299.

[29] C. A. Balanis, *Antenna Theory Analysis and Design*, 3rd ed. Hoboken, NJ, USA: Wiley, 2005.

[30] S. R. Saunders and A. Aragon-Zavala, *Antennas and Propagation for Wireless Communication Systems*, 2nd ed. West Sussex, U.K.: Wiley, 2007.

[31] F. Bohagen, P. Orten, and G. E. Oien, "Design of Capacity-Optimal High-Rank Line-Of-Sight MIMO Channels," Univ. Oslo, Oslo, Norway, Res. Rep. 352, Mar. 2007.

[32] F. Bohagen, P. Orten, and G. E. Oien, "Modeling of line-of-sight 2x2 MIMO channels spherical versus plane waves.," in *Proc. IEEE PIMRC*, Helsiniki, Finland, Sep. 2006, pp. 1–5.

[33] T. Zwick, C. Fischer, D. Didascalou, and W. Wiesbeck, "A stochastic spatial channel model based on wave-propagation modeling," *IEEE J. Sel. Areas Commun.*, vol. 18, no. 1, pp. 6–15, Jan. 2000.

[34] T. Zwick, C. Fischer, and W. Wiesbeck, "A stochastic multipath channel model including path directions for indoor environments," *IEEE J. Sel. Areas Commun.*, vol. 20, no. 6, pp. 1178–1192, Aug. 2002.

[35] C. C. Chong, C. M. Tan, D. I. Laurenson, S. McLaugnlin, and M. A. Beach, "A novel wideband dynamic directional indoor channel model based on a Markov process," *IEEE Trans. Wireless Commun.*, vol. 4, no. 4, pp. 1539–1552, Jul. 2005.

[36] F. Babich and G. Lombardi, "A Markov model for the mobile propagation channel," *IEEE Trans. Veh. Technol.*, vol. 48, no. 1, pp. 63–73, Jan. 2000.

[37] D. S. Baum, J. Hansen, and J. Salo, "An interim channel model for beyond-3G systems: Extending the 3GPP spatial channel model (SCM)," in *Proc. IEEE VTC–Spring*, Stockholm, Sweden, May 2005, vol. 5, pp. 3132–3136.

[38] H. Xiao, A. G. Burr, and L. Song, "A time-variant wideband spatial channel model based on the 3GPP model," in *Proc. IEEE VTC–Fall*, Montreal, Canada, Sep. 2006, pp. 1–5.

[39] S. Wu, C.-X. Wang, and H. Aggoune, "Non-stationary wideband channel models for massive MIMO systems," in *Proc. WSCN*, Jeddah, Saudi Arabia, Dec. 2013, pp. 1–8.

[40] S. Wu, C.-X. Wang, el-H. M. Aggoune, M. M. Alwakeel, and Y. He, "A non-stationary 3-D wideband twin-cluster model for 5G massive MIMO channels," *IEEE J. Sel. Areas Commun.*, vol. 32, no. 6, pp. 1207–1218, Jun. 2014.

[41] A. Abdi, J. A. Barger, and M. Kaveh, "A parametric model for the distribution of the angle of arrival and the associated correlation function and power spectrum at the mobile station," *IEEE Trans. Veh. Technol.*, vol. 51, no. 3, pp. 425–434, May 2002.

[42] X. Cheng *et al.*, "Wideband channel modeling and ICI cancellation for vehicle-to-vehicle communication systems," *IEEE J. Sel. Areas Commun.*, vol. 31, no. 9, pp. 434–448, Sep. 2013.

[43] A. Abdi and M. Kaveh, "A space-time correlation model for multielement antenna systems in mobile fading channels," *IEEE J. Sel. Areas Commun.*, vol. 20, no. 3, pp. 550–560, Apr. 2002.

[44] Y. Chen and V. K. Dubey, "Dynamic simulation model of indoor wideband directional channels," *IEEE Trans. Veh. Technol.*, vol. 55, no. 2, pp. 417–430, Mar. 2006.

[45] A. Papoulis and S. U. Pillai, *Probability, Random Variables, Stochastic Processes*, 4th ed. New York, NY, USA: McGraw-Hill, 2002.

[46] L. C. Godara, "Application of antenna arrays to mobile communications Part II: Beam-forming and direction-of-arrival considerations," *Proc. IEEE*, vol. 85, no. 8, pp. 1195–1245, Aug. 1997.

[47] A. F. Molisch, *Wireless Communications*, 2nd ed. West Sussex, U.K.: Wiley, 2005.

Shangbin Wu received the Bachelor's degree in communication engineering from South China Normal University, Guangzhou, China, in 2009 and the M.Sc. degree (with distinction) in wireless communications from University of Southampton, U.K., in 2010. He is pursuing the Ph.D. degree at Heriot-Watt University, Edinburgh, U.K., since 2012. He worked as an LTE R&D Engineer responsible for LTE standardization and system level simulation at New Postcom Equipment Ltd., Guangzhou, from 2010 to 2011. From October 2011 to August 2012, he was with Nokia Siemens Network where he worked as an LTE Algorithm Specialist, mainly focusing on LTE Radio Resource Management (RRM) algorithm design and system level simulations. His research interests include wireless channel modeling and simulation, spatial modulation, and massive multiple-input multiple-output (MIMO) systems.

Cheng-Xiang Wang (S'01–M'05–SM'08) received the B.Sc. and M.Eng. degrees in communication and information systems from Shandong University, Shandong, China, in 1997 and 2000, respectively, and the Ph.D. degree in wireless communications from Aalborg University, Aalborg, Denmark, in 2004. Since 2005, he has been with Heriot-Watt University, Edinburgh, U.K., and was promoted to Professor in 2011. He is also an Honorary Fellow of the University of Edinburgh and a Chair/Guest Professor with Shandong University and Southeast University, China. From 2001 to 2005, he was a Research Fellow with the University of Agder, Grimstad, Norway. In 2004, he was a Visiting Researcher with Siemens AG-Mobile Phones, Munich, Germany. From 2000 to 2001, he was a Research Assistant with the Technical University of Hamburg-Harburg, Hamburg, Germany. He is the Editor of one book. He has published one book chapter and over 200 papers in refereed journals and conference proceedings. His research interests include wireless channel modeling and simulation, green communications, cognitive radio networks, vehicular communication networks, massive multiple-input multiple-output (MIMO), and fifth-generation (5G) wireless communications.

Prof. Wang is a Fellow of the Institution of Engineering and Technology and the HEA and a member of the Engineering and Physical Research Council Peer Review College. He has served as an Editor for eight international journals, including the IEEE TRANSACTIONS ON VEHICULAR TECHNOLOGY (since 2011) and the IEEE TRANSACTIONS ON WIRELESS COMMUNICATIONS (2007–2009). He was the lead Guest Editor for the IEEE JOURNAL ON SELECTED AREAS IN COMMUNICATIONS, Special Issue on Vehicular Communications and Networks. He has served as a Technical Program Committee (TPC) Member, TPC Chair, and General Chair for more than 70 international conferences. He received the Best Paper Awards from IEEE Globecom 2010, IEEE ICCT 2011, ITST 2012, and IEEE VTC 2013-Spring.

Harald Haas (S'98–AM'00–M'03) received the Ph.D. degree from the University of Edinburgh, Edinburgh, U.K., in 2001. He currently holds the Chair of Mobile Communications at the University of Edinburgh. His main research interests are in optical wireless communications, hybrid optical wireless and RF communications, spatial modulation, and interference coordination in wireless networks. He first introduced and coined spatial modulation and Li-Fi. Li-Fi was listed among the 50 best inventions in *TIME Magazine* 2011. He was an invited speaker at TED Global 2011, and his talk has been watched online more than 1.5 million times. He is Co-founder and Chief Scientific Officer (CSO) of pure LiFi Ltd. He holds 31 patents and has more than 30 pending patent applications. He has published 300 conference and journal papers including a paper in *Science*. He was co-recipient of a Best Paper Award at the IEEE Vehicular Technology Conference in Las Vegas, NV, USA, in 2013. In 2012, he was the only recipient of the prestigious Established Career Fellowship from the Engineering and Physical Sciences Research Council (EPSRC) within Information and Communications Technology in the UK. He is recipient of the Tam Dalyell Prize 2013 awarded by the University of Edinburgh for excellence in engaging the public with science. In 2014, he was selected by EPSRC as one of ten Recognising Inspirational Scientists and Engineers (RISE) Leaders.

el-Hadi M. Aggoune (M'83–SM'93) received the M.S. and Ph.D. degrees in electrical engineering from the University of Washington (UW), Seattle, WA, USA. He is a Professional Engineer registered in the State of Washington, He served at a number of universities in the US and abroad. The highest academic ranks he achieved included Endowed Chair Professor and Vice President and Provost. He managed a research lab that won the Boeing Supplier Excellence Award. He was a winner of the IEEE Professor of the Year Award, UW Branch. He is listed as Inventor in a major patent assigned to the Boeing Company. His research work is referred to in many patents including patents assigned to ABB, Switzerland and EPRI, USA. Currently, he is a Professor and Director of the Sensor Networks and Cellular Systems (SNCS) Research Center, University of Tabuk, Tabuk, Saudi Arabia. He has authored papers in IEEE and other journals and conferences. He currently serves on many technical committees. His research interests include modeling and simulation of large scale networks, sensors and sensor networks, scientific visualization, and control and energy systems.

Mohammed M. Alwakeel (SM'14) was born in Tabuk, Saudi Arabia, in 1970. He received the B.S. degree in computer engineering and the M.S. degree in electrical engineering from King Saud University, Riyadh, Saudi Arabia, in 1993 and 1998, respectively, and the Ph.D. degree in electrical engineering from Florida Atlantic University, Boca Raton, FL, USA, in 2005. From 1994 to 1998, he was a Communications Network Manager at The National Information Center, Saudi Arabia. From 1999 to 2001, he was with King Abdulaziz University, Jeddah, Saudi Arabia. From 2009 to 2010, he was an Associate Professor and the Dean of the College of Computers and Information Technology, University of Tabuk. He is currently the Vice Rector for Development and Quality of the University of Tabuk. His current research interests include teletraffic analysis, mobile satellite communications, sensor networks, and cellular systems.

Bo Ai (M'00–SM'10) received the M.S. and Ph.D. degrees from Xidian University, Xian, China, in 2002 and 2004, respectively. He was with Tsinghua University, Beijing, China, where he was an Excellent Postdoctoral Research Fellow in 2007. He is currently a Professor and an Advisor of Ph.D. candidates with Beijing Jiaotong University, Beijing, where he is also the Deputy Director of the State Key Laboratory of Rail Traffic Control and Safety. He is also currently with the Engineering College, Armed Police Force, Xian. He has authored or coauthored six books and 160 scientific research papers, and holds 26 invention patents in his research areas. His interests include the research and applications of orthogonal frequency-division multiplexing techniques, high-power amplifier linearization techniques, radio propagation and channel modeling, global systems for mobile communications for railway systems, and long-term evolution for railway systems.

Dr. Ai is a Fellow of The Institution of Engineering and Technology. He was as a Cochair or a Session/Track Chair for many international conferences such as the 9th International Heavy Haul Conference (2009); the 2011 IEEE International Conference on Intelligent Rail Transportation; HSRCom2011; the 2012 IEEE International Symposium on Consumer Electronics; the 2013 International Conference on Wireless, Mobile and Multimedia; IEEE Green HetNet2013; and the IEEE 78th Vehicular Technology Conference (2014). He is an Associate Editor of IEEE TRANSACTIONS ON CONSUMER ELECTRONICS and an Editorial Committee Member of the *Wireless Personal Communications journal*. He has received many awards such as the Qiushi Outstanding Youth Award from the Hong Kong Qiushi Foundation, the New Century Talents from the Chinese Ministry of Education, the Zhan Tianyou Railway Science and Technology Award from the Chinese Ministry of Railways, and the Science and Technology New Star from the Beijing Municipal Science and Technology Commission.